Response scenario and non-smooth features in the nonlinear dynamics of an impacting inverted pendulum

Stefano Lenci
Dipartimento di Architettura, Costruzioni e Strutture
Università Politecnica delle Marche, Ancona, Italy
Lenci@univpm.it

Lucio Demeio, Milena Petrini
Dipartimento di Scienze Matematiche
Università Politecnica delle Marche, Ancona, Italy
L.Demeio@univpm.it, M.Petrini@univpm.it

April 14, 2005

Abstract

In this work, we perform a systematic numerical investigation of the nonlinear dynamics of an inverted pendulum between lateral rebounding barriers. Three different families of considerably variable attractors, periodic, chaotic, and rest positions with subsequent chattering, are found. All of them are investigated in detail, and the response scenario is determined by both bifurcation diagrams and behaviour charts of single attractors, and overall maps. Attention is focused on local and global bifurcations that lead to the attractors-basins metamorphoses. Numerical results show the extreme richness of the dynamical response of the system, which is deemed to be of interest also in view of prospective mechanical applications.

Keywords. Inverted pendulum, non-smooth dynamics, chattering, chaos, impact damper.

1 Introduction

In this work, a detailed analysis of the nonlinear dynamics of an inverted pendulum bouncing on lateral walls (Figure 1) is performed. The study of this system has both practical and theoretical motivations.

The inverted pendulum is used in the modelling of several engineering applications, such as rings, printers, machine tools, dynamics of rigid standing structures, mooring buoy, moored vessels in a harbour against stiff fenders, rolling railway wheelset [6]. Impact oscillators have also applications in the emerging field of micro electro-mechanical systems (MEMS) [22]. Furthermore, one promising application is in the field of impact dampers, which are nowadays used in several fields, including mechanical and civil applications, to reduce high-amplitude vibrations.

The mechanisms of protection consist of energy dissipation or of frequency shifting, and impact dampers are sometimes preferred to classical viscous dampers due to their simplicity and easyness of maintenance. Examples of structures which can be safely protected by impact dampers are cutting tools [16], turbine blades, tall flexible structures like chimneys, antennas, traffic-lights, scaffolding.

As noted in [2], "*Despite several advantages...the use of a passive impact damper is limited due to its ineffectiveness for broadband excitation.*" To overcome this limitation, control of the dynamics of impact dampers has been proposed [2, 11]. An impact damper based on the inverted pendulum is instead able to overcome the previous drawback still through a *passive* mechanism. In fact, it has no internal frequencies, so it can work well, at least in principle, in a broad range of frequencies.

Another characteristic is that it has an activation threshold before it starts to dissipate, below which the pendulum rests on the lateral barrier. This means that it works only when the vibrations of the main structure overcome a certain threshold, namely, it comes into play only when necessary.

The previous properties are very useful in applications, and call for an extended analysis of the dynamical response of the system, which is the main objective of the present work. However, this is not the only motivation for this analysis. In fact, the inverted pendulum represents an archetype of a family of impacting oscillators whose dynamics possesses some specific phenomena, such as chattering [1] and multistability, which are of theoretical interest *per se*.

It is worth noting that the well known "grazing" bifurcation [13], which

is relevant to many non-smooth systems [14], is not peculiar here, because of the negative stiffness. The role of grazing in characterizing the non-smooth response is here assumed by chattering.

While the dynamics of the "free" inverted pendulum has been largely investigated, especially with regard to the stabilization of the unstable solutions, which became a classical after Stephenson [20], the dynamics of the inverted pendulum between lateral walls has received minor attention.

The existence and the stability of two classes of periodic solutions were studied analytically in [17] and their relation with the route to chaos established by the Melnikov's method was discussed. That work was accompanied by an extensive experimental investigation [12] aimed at checking some of the theoretical results.

Successively, it was suggested [18] to modify the shape of the excitation in order to avoid homoclinic intersection and, consequently, to control the chaotic dynamics of the system. Shaw looked for the solution in a restricted class of excitations. The optimization problem was generalized and solved in [7], where it was found that the optimal periodic excitation is constituted by two equal and opposite impulses plus a bounded part. The two-impulse approximation of the optimal excitation has been numerically checked in [8], where various specific aspects of control were addressed and also the ensuing dynamics was compared with those of the reference harmonic excitation.

The previous numerical analysis was accompanied by a theoretical work [9], where some aspects of the nonlinear dynamics were detected analytically. In particular, the same class of periodic solutions studied in [17] was investigated, but with the two-impulsed instead of the harmonic excitation. It was shown that they undergo both classical saddle-node and period-doubling bifurcations and "nonclassical" bifurcations involving a synchronization between impulses and impacts on lateral barriers.

A theoretical investigation of the inverted pendulum with an *arbitrary* periodic excitation, i.e. without restricting the analysis to the harmonic or to the two-impulse excitation, was accomplished in [10], following the same lines of [17] and [9]. This analysis was motivated by the fact that general periodic excitations have been proposed for controlling nonlinear dynamics and chaos and that they appear in many practical applications, for example because of the nonlinear coupling with other structures.

All the theoretical works that we have quoted, apart from those devoted to the control of chaos, basically consider a class of periodic solutions bouncing one time in each period of the motion, under various excitations. In

particular, they study the appearance and disappearance of these attractors through classical and non-classical local bifurcations. This class of orbits is very important and usually includes the predominant attractor, but it does not cover the whole family of possible attractors.

In order to explore the whole dynamical response, extensive numerical simulations are required. Some of them are reported in [8], but, since those works were aimed at studying the effect of control and not of the overall dynamics, they considered only a fixed value of the excitation frequency, and studied in depth only the effects of the excitation amplitude. In this paper, we extend those studies by performing systematic numerical simulations on the *whole* frequency-amplitude parameters plane.

While extending the results of [8], this work considers only harmonic excitation, in order to limit the lenght of the paper. Extensive numerical simulations with non-harmonic excitation are left for future work.

The paper is organized as follows. After the mathematical model of the pendulum described in Section 2, the three main classes of system responses are investigated separately: periodic attractors (Section 3), chattering (Section 4) and robust chaotic attractors (Section 5). In Section 6 we state our conclusions, together with open problems and plans for future work.

2 The model

The nonlinear dynamics of the inverted pendulum between lateral walls (Figure 1) is described by the equations [7]

$$\begin{array}{ll} \ddot{x} + 2\delta\dot{x} - x = \gamma\sin(\omega t), & |x| < 1, \\ \dot{x}(t^+) = -r\dot{x}(t^-), & |x| = 1, \end{array} \tag{1}$$

where $x = \theta/\theta_{max}$ is the normalized angle (Figure 1), δ is the viscosity coefficient ($0 < \delta < 1$), $f(t) = \gamma\sin(\omega t)$ is the harmonic excitation representing the horizontal acceleration of the base, t^- and t^+ are the instants of time immediately before and after an impact and r is the restitution coefficient ($0 < r \leq 1$, $r = 1$ for elastic impacts).

The equation which is obtained from (1) by switching off the excitation will be referred to as the *unforced* problem. By further setting $\delta = 0$ and $r = 1$, we obtain a *conservative* system, corresponding to an undamped impact pendulum undergoing elastic collisions with the walls, to which we

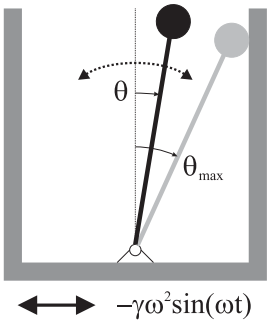

Figure 1: The impacting inverted pendulum.

associate the potential energy

$$\begin{aligned} V(x) &= -\tfrac{x^2}{2}, \quad |x| < 1, \\ V(x) &= \infty, \qquad |x| = 1, \end{aligned} \tag{2}$$

which can be thought of as being comprised of two potential wells, one on the left and one on the right of the *hilltop saddle* at $x = 0$. The phase portrait is shown in Figure 2, where we recognize a class of scattered periodic orbits, which correspond to energies above $V(0)$, and a class of confined periodic orbits, occurring either in the left well or in the right well. This classification of the orbits survives also when the excitation force is added.

The two classes of motion are divided by the homoclinic loops of the hilltop saddle (thick lines of Figure 2), and are seen to play an important role in the sequel.

In the presence of damping, there are only two attractors: $x = \pm 1$. Adding the excitation generates a very rich dynamical behaviour, comprising many attractors. In the following, we identify and study in depth three classes of attractors: periodic attractors, rest position and subsequent chattering oscillations, and robust chaotic attractors. As they cannot be detected analytically (apart from few of them), this work is aimed at carrying out a systematic *numerical* analysis by studying the onset and the evolution of the attractors as the parameters ω and γ are varied, as well as their specific properties.

In all our numerical solutions, we have taken $\delta = 0.05$ and $r = 0.92$, which are reasonable values in many practical applications.

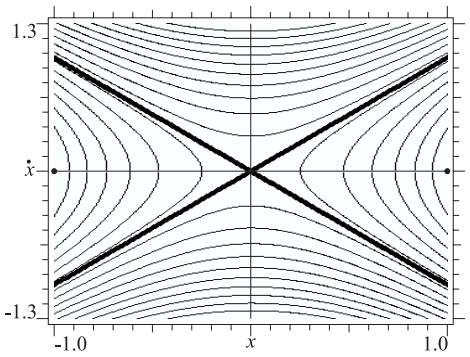

Figure 2: The phase space portrait for the conservative system.

3 Periodic response scenario and multistability

In this section we describe and classify the main periodic attractors which we have detected in our analysis. Each periodic attractor is classified according to its period (in units of $T = 2\pi/\omega$, the period of the excitation force), to the number of impacts with the walls per period of the motion and to its being confined to one of the wells of the potential $V(x)$ (confined attractor) or not (scattered attractor).

With this criterion, first introduced in [14], each attractor is labeled like $n-m-x$, n being the period of the motion (in units of T), m the number of impacts per period with the walls and x=c or s, the indicator of a confined or scattered attractor, respectively. Note that $n-1-c$ and a subclass of (symmetric) $n-2-s$ attractors were detected analytically in [17] and [10].

It is worth remarking that for each confined attractor $x(t)$ there exists a specular one $x_1(t) = -x(t+T/2)$. The scattered solutions, on the other hand, can be self-symmetric or, alternatively, they also have their symmetric counterpart. This property no longer holds if the excitation contains even superharmonic terms.

In Figures 3a and 3b, and 4a and 4b, we show examples of some confined and some scattered attractors, respectively. Figures 3a and 4a show the phase-space orbits of the attractors, while Figures 3b and 4b show the relevant time histories.

The attractors of Figure 3 are clearly confined to the right well, have

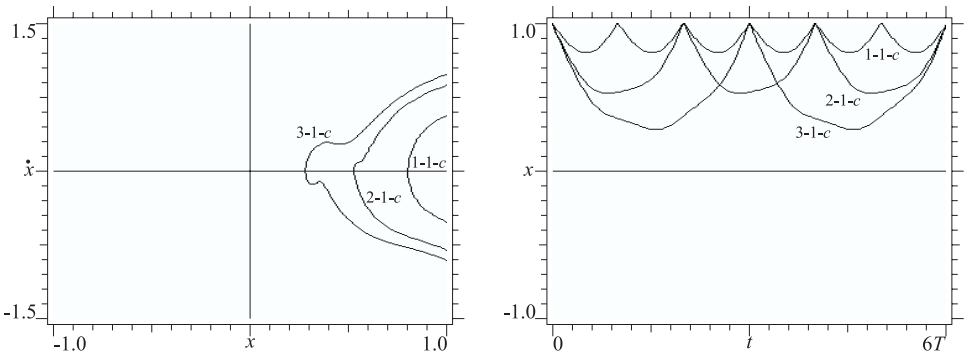

a) b)

Figure 3: Three confined periodic attractors for $\omega = 5$ and $\gamma = 0.5$. a) Phase portraits; b) time histories.

period 1, 2 and 3, and suffer one impact with the wall per period. The attractors of Figure 4 are scattered, have period 1, 2 and 3 and suffer two impacts per period with the walls.

Typically, as one parameter is varied, at some value a confined periodic attractor is born by a saddle-node bifurcation. When the parameter is varied further, the attractor loses stability at a certain threshold by a period doubling bifurcation, and then a period doubling cascade follows, which eventually ends in a chaotic attractor. This attractor, which has a small extention in the phase space, survives for a certain range, usually very small, of the control parameter, and then suddenly disappears through a crisis. An example is reported in Figure 5.

The behaviour of scattered attractors is quite similar, the main difference being that when the periodic orbit, born by a saddle-node bifurcation, is self-symmetric, it first undergoes a pitchfork (or simmetry breaking) bifurcation before the period doubling cascade which leads to the chaotic attractor and then to the crisis. A typical example is reported in Figure 6.

All of the periodic attractors which we have detected numerically by varying the initial conditions show this kind of behaviour. They are: $1-1-c$, $1-2-c$, $1-3-c$, $2-1-c$, $3-3-c$, $1-2-s$, $1-4-s$, $3-2-s$, $3-6-s$, $1-3-s$ and $2-6-s$. Bifurcation diagrams such as those of Figures 5 and 6 have been constructed systematically for each of these attractors. This

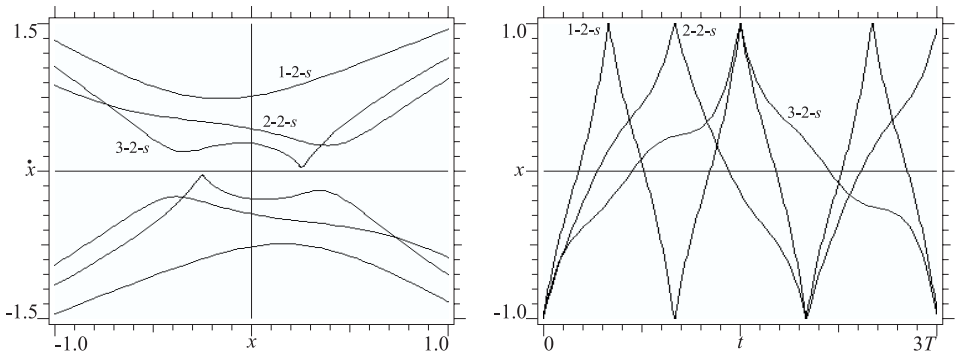

a) b)

Figure 4: Three scattered periodic attractors for $\omega = 1.5$ and $\gamma = 0.4$. a) Phase portraits; b) time histories.

permits to construct behaviour charts like those of Figure 7, where the loci of SN bifurcation (lower curve), PD or PF bifurcation (middle curve) and final crisis (upper curve) are reported in the parameter space (ω,γ) with reference to a $1-1-c$ and a $1-2-s$ attractor.

Figure 7 provides the regions of stability of the periodic attractors, as well as the subsequent regions of route to chaos. A common feature observed in the behaviour charts of all attractors is that the region of existence collapses for $\omega \to 0$, while they enlarge for $\omega \to \infty$.

Charts like those of Figure 7 have been determined analytically in [17] for $n-1-c$ and for $n-2-s$ self-symmetric attractors. They are here systematically extended to more general periodic orbits, and the final crisis, which can be determined only numerically, is also detected.

For each given value of ω and γ, several periodic attractors can coexist, each of them with its own basin of attraction. This is the phenomenon of multistability, which is illustrated in Figure 8, where we show the variable number of periodic attractors coexisting in various regions within the range $0.5 \leq \omega \leq 5$ and $0 \leq \gamma \leq 2$ (rest positions and chaotic attractors are not reported). This map is obtained by superposing all behaviour charts like those of Figure 7, and shows how the multistability phenomenon is important in the lower right part of the map, i.e., for relatively large frequencies and relatively small amplitudes. On the upper right part the only periodic

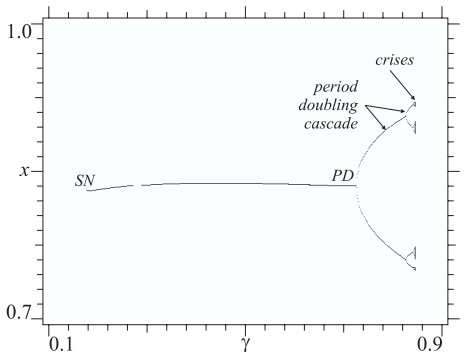

Figure 5: A typical bifurcation diagram for confined attractors. $\omega = 5.0$.

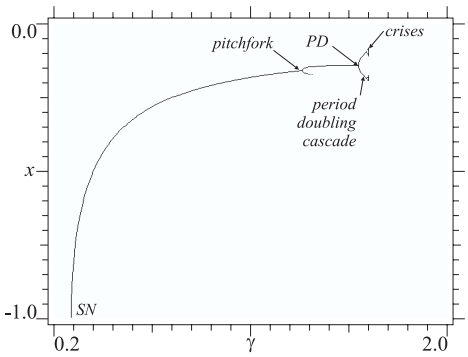

Figure 6: A typical bifurcation diagram for scattered attractors. $\omega = 1.5$.

attractor is a self-symmetric $1-2-s$, which is the one reported in Figure 4.

An example of multistability is portrayed in Figure 9, which reports the basins of attraction of the coexisting *nine* attractors. They are the two left and right rest positions (because we are below $\gamma = 1$, see Sect. 4) and seven periodic attractors, which are two $1-1-c$ (one and its symmetric), two $1-2-c$, two $3-3-c$ and one $3-2-s$ (characterized by the white basin of attraction).

Apart from the very high number of coexisting attractors, it is remarkable that not only rest positions and periodic orbits coexist, but also that both scattered and confined attractors coexist (and compete with each other). Moreover, as we shall see in Sect. 5, also robust chaotic and periodic attractors do coexist. These observations, and the consideration that the coexistence of various attractors occurs on an extended region of the parameter space, permit to conclude that multistability is a very important dynamical feature of this dynamical system.

Associated with multistability, is the strongly fractal nature of the basins of attraction, which is also evident in Figure 9. This is likely due to the combined effects of the homoclinic and heteroclinic intersections between the saddles associated with the various periodic attractors and the hilltop saddle (note that the homoclinic bifurcation of the hilltop saddle occurs for a lower value of the excitation amplitude). In fact, we conjecture that it is the tangle created by these repeated and multiple intersections which is at the basis of the observed fractality.

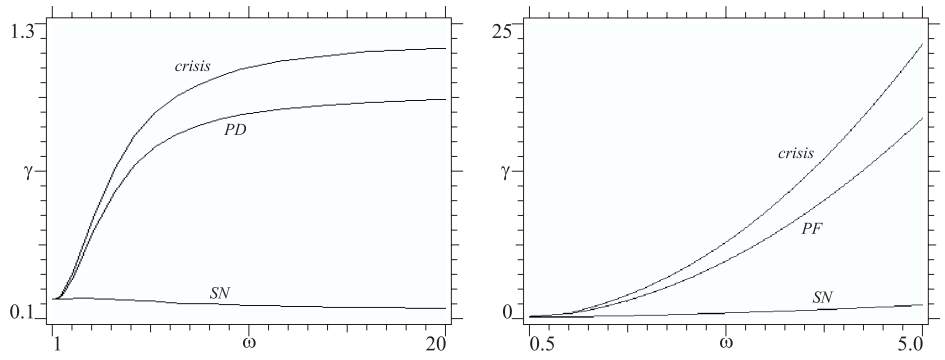

a) b)

Figure 7: The behaviour chart for a) a $1-1-c$ attractor and b) a $1-2-s$ attractor.

The extended fractal nature contributes to increase the complexity of the behaviour and to increment unpredictability. This represents the high sensitivity of the system to initial conditions, and should be carefully taken into account in practical applications. Indeed, none of the attractors of Figure 8 is safe from an engineering point of view, because of the small extent of each basin of attraction.

4 Chattering oscillations

In this section we focus our attention on the phenomenon which follows the loss of existence and stability of the rest positions at $x = \pm 1$.

For the conservative case, $x = \pm 1$ are stable centers, although of a quite unusual nature, because they have surrounding orbits only on one side of the phase space (see Figure 2). When the exitation force is introduced, they remain stable as long as $\gamma < 1$; at $\gamma = 1$ they disappear and, for values of γ slightly larger than 1, an interesting phenomenon, called *chattering*, occurs.

Chattering was previously investigated in the literature [1], and it appears as a source of undesired dynamics in many engineering applications, such as metal cutting [21].

To shortly explain the phenomenon, suppose that the system is initialized at the left rest position $x = -1$ with $\dot{x} = 0$. As long as the total force F

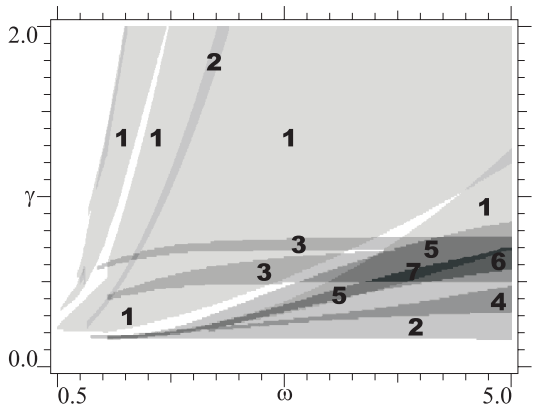

Figure 8: Map of coexisting periodic attractors.

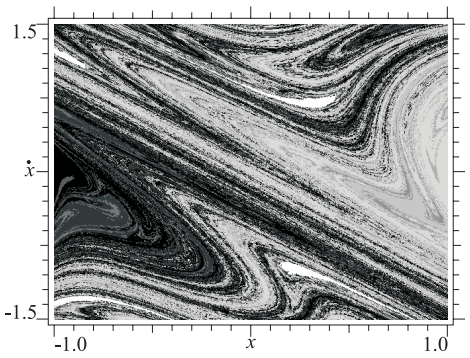

Figure 9: Basins of attraction for $\omega = 4.4$ and $\gamma = 0.61$.

acting on the mass (sum of the gravity and of the excitation) keeps pushing the pendulum towards the wall for all times, the system doesn't move. This occurs as long as $F = -1 + \gamma sin(\omega t) < 0$ for all $t > 0$, i.e., for $\gamma < 1$. Above this threshold, there is a time interval in which the force pulls the mass away from the wall; for $\gamma \approx 1$ this time interval is short, and the excitation force is not strong enough to overcome gravity and to pull the mass far away from the wall: a high-frequency, low-amplitude oscillatory motion is then observed, in which the pendulum repeatedly hits the wall.

These chattering oscillations are characterized by a very small amplitude, which decreases in time, as shown in Figure 10, and are constituted by an

infinite number of impacts occurring in a finite time, called chattering time τ, which is a fraction of the excitation period. Because of the small amplitude, they are also referred to as *micro*-oscillations. They eventually die away after a time interval of τ (Figure 10), and the mass remains motionless on the wall until, in the next period, the excitation is again (slightly) larger than gravity, and the phenomenon appears again. Indeed, as confirmed by the examples of Figure 10, chattering oscillations develop and die entirely within a single period of the excitation.

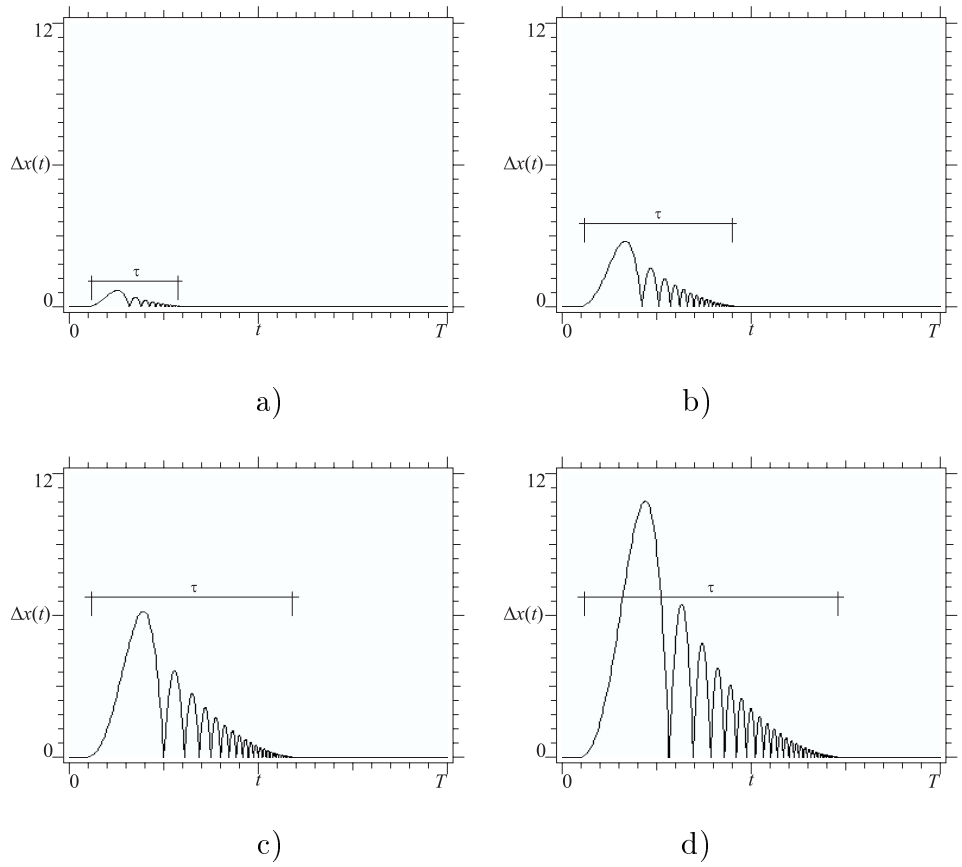

Figure 10: Chattering oscillations. $\Delta x(t) \equiv (1 + x(t))10^4$ as a function of t, for $\omega = 5$ and a) $\gamma = 1.02$, b) $\gamma = 1.04$, c) $\gamma = 1.06$ and d) $\gamma = 1.08$.

The effect of increasing γ from 1 is also illustrated in Figure 10. We see that the amplitude of the oscillations and the chattering time both increase

with γ, the former remaining always small. It follows that at a certain critical value γ_{cr}^c, the chattering time τ equals the excitation period. This is the final event representing the destruction of chattering. Then, after a certain transient, usually quite long, the solution approaches another attractor, which may or may not coexist with chattering for $1 < \gamma < \gamma_{cr}^c$.

Due to its nature, chattering is extremely difficult to be detected numerically. For this reason, an accurate numerical estimate of $\tau = \tau(\gamma)$ and, consequently, of the excitation amplitude γ_{cr}^c, is very hard to obtain. To overcome this difficulty, a pseudo-analytical method is suggested. It is based on the observation that the ratio $\Delta t_{i+1}/\Delta t_i$ tends to the restitution coefficient r as $i \to \infty$. Here, Δt_i is the time interval between two consecutive impacts. This property is shown in Figure 11, which reports the ratio $\Delta t_{i+1}/\Delta t_i$ as a function of i for a fixed frequency and for various values of γ.

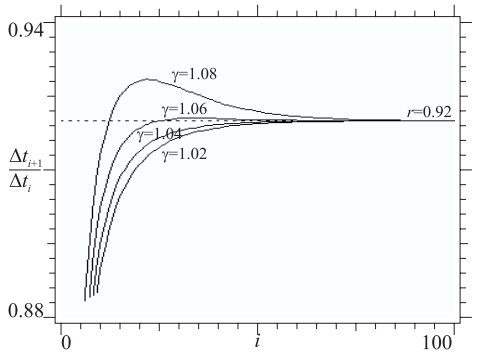

Figure 11: The ratio $\Delta t_{i+1}/\Delta t_i$ as a function of the impact sequential number i for $\omega = 5$.

From the previous considerations, we obtain that for $i > n$, with n sufficiently large,

$$\Delta t_i \cong r^{i-n} \Delta t_n. \tag{3}$$

Therefore,

$$\tau = \sum_{i=1}^{\infty} \Delta t_i = \sum_{i=1}^{n-1} \Delta t_i + \sum_{i=n}^{\infty} \Delta t_i \cong \sum_{i=1}^{n-1} \Delta t_i + \frac{\Delta t_n}{1-r}, \tag{4}$$

which leaves only the first n impact times to be computed numerically. Note that this method requires n sufficiently large (see Figure 11), and it can be

chosen by checking that $\Delta t_{n+1}/\Delta t_n$ is close enough to r. After this value has been identified, eq. (4) can then be easily applied to get the desired τ for each value of γ.

An example of computation of the function $\tau(\gamma)$ is reported in Figure 12. Apart from confirming that $\tau(\gamma)$ is increasing, as noted in Figure 10, this picture permits to estimate γ_{cr}^c by direct inspection. In this case, we get $\gamma_{cr}^c \cong 1.1$. However, this estimate is not very accurate because, as γ approaches γ_{cr}^c, the computed value of τ becomes less and less accurate. In spite of this, however, this estimate allows to conclude that the γ range of existence of chattering is quite small.

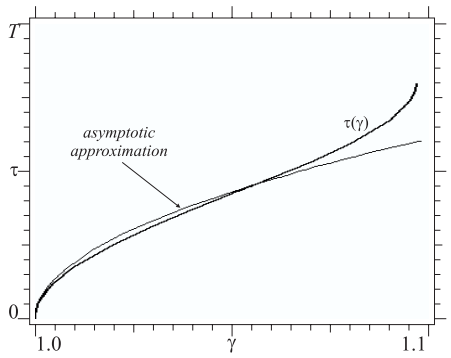

Figure 12: The function $\tau(\gamma)$ and its asymptotic approximation for $\omega = 5$.

Remark 1. Because of the very small amplitude of the chattering oscillations and of the small range of γ in which chattering occurs, it is possible that the phenomenon is entirely missed in the numerical simulations, if they are not carried out with sufficient accuracy. In that case, it is possible to attribute the end of the attractor close to the wall to the end of the rest position ($\gamma = 1$) while it should, more correctly, be attributed to the end of the chattering oscillations. From an engineering point of view, however, this error may or may not be of interest in practical applications.

Figure 12 shows that the curve $\tau(\gamma)$ has singular derivatives at both ends. The singularity at $\gamma \approx \gamma_{cr}^c$ is at the basis of the numerical difficulties encountered in the computation of γ_{cr}^c; the singularity for $\gamma \to 1$ is studied in detail in [3], by an accurate asymptotic expansion of the relevant quantities.

It is shown there that, for $\gamma \to 1$,

$$\tau(\gamma) \cong \frac{S}{\omega}\sqrt{2}\sqrt{\gamma - 1}, \tag{5}$$

which shows that the function $\tau(\gamma)$ has a square root singularity at $\gamma = 1$. Here, the number S depends only on r and is given by

$$S = \sum_{n=0}^{\infty} c_n r^n, \tag{6}$$

the coefficients c_n being defined recursively by $c_0 = 4$ and by

$$c_n = \frac{32}{3}\left[\left(\sum_{k=0}^{n-1} c_k r^k - 1\right)^2 - 1\right]^{-1}. \tag{7}$$

For $r = 0.92$ (the value used in this work) we have $S = 8.58267$. The corresponding asymptotic approximation of $\tau(\gamma)$ is reported in Figure 12. Apart from the excellent agreement for $\gamma \to 1$, this picture shows that the asymptotic estimate provides a good approximation of the chattering time also for relatively large values of γ. Indeed, quite surprisingly, eq. (5) seems to be inaccurate only for $\gamma \to \gamma_{cr}^c$, at least in the considered example.

5 Robust chaotic attractors, crises and global bifurcations

The periodic attractors, the rest attractors and the chattering oscillations are not the only attractors exhibited by the system dynamics. Indeed, robust chaotic attractors have also been repeatedly observed. Here, robust means chaotic attractors which have a non small extention in the phase space and that persist for sufficiently large variations of the parameters. Practically, they are not the (small) chaotic attractors appearing at the end of the period doubling cascade. Examples of confined and scattered robust chaotic attractors are shown in Figures 18a and 18b, respectively. In the following we refer only to robust chaotic attractor, so that the adjective "robust" is omitted for brevity.

As in Sect. 3, chaotic attractors are studied by the combined used of bifurcation diagrams and basins of attraction. Examples of bifurcation diagrams for "small" and "large" frequencies are reported in Figure 13a and 13b, respectively.

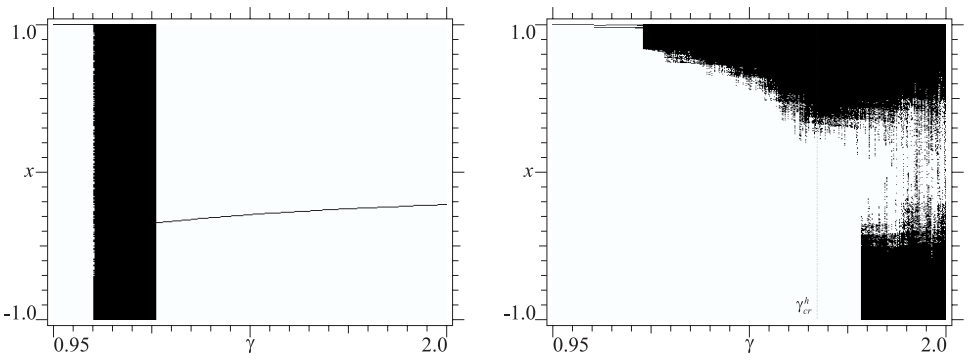

a) b)

Figure 13: Bifurcation diagrams for a) $\omega = 3$ and b) $\omega = 18$.

In the case of Figure 13a, after the end of the chattering oscillations, the solution approches a scattered chaotic attractor just established on the skeleton of the chaotic saddle created by the homoclinic bifurcation of the hilltop at $\gamma^h_{cr} = 0.3057$ (see eq. (8)). When the governing parameter grows further, the scattered chaotic attractor enlarges inside its basin until, for $\gamma \cong 1.222$ it touches the basin boundary and disappears (curve (A) of Figure 14). Successively, a periodic attractor previously coexisting with the chaotic attractor becomes globally attracting.

In the case of large frequency (Figure 13b), after the end of the chattering motion, the solution jumps onto a previously coexisting periodic attractor, belonging to the PD cascade of the $1-1-c$ periodic attractor of Figure 7a, and experiencing a classical route to chaos (curve (C) of Figure 14). This path ends with a crisis at about $\gamma \cong 1.19$ after which a *confined* chaotic attractor is established. When the governing parameter grows further, the confined chaotic attractor enlarges inside its basin until, for $\gamma = \gamma^h_{cr} = 1.656$ (see eq. (8)) it touches the basin boundary, and merges with its symmetric counterpart giving a unique *scattered* chaotic attractor (curve (D) of Figure 14).

From the comparison of Figures 13a and 13b, we see that (i) no chaotic attractors are observed below γ_{cr}^{c} and (ii) confined chaotic attractors occur only for large frequencies. To confirm these observations, many bifurcation diagrams have been constructed sistematically, and the behaviour chart of Figure 14 has been obtained, where the regions of existence of confined and scattered chaotic attractors are reported.

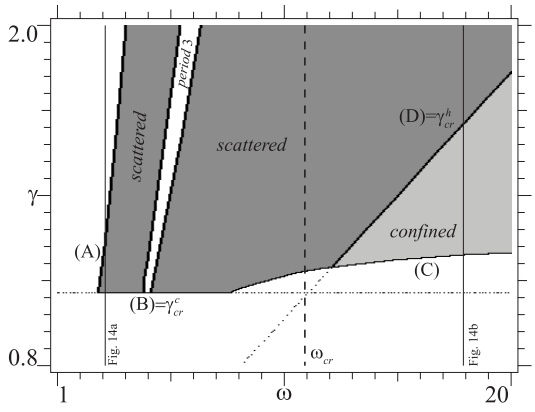

Figure 14: Map of robust chaotic attractors.

The regions of Figure 14 are delimited by four main curves, which are now discussed.

Curve (A). On the right of curve (A), the chaotic attractor is not unique (Figure 15) and coexists with the scattered $1-2-s$ self-symmetric periodic attractor of Figure 7b. As the governing parameter approaches curve (A), the scattered chaotic attractor enlarges inside its basin until, at (A), it touches the basin boundary, as shown by the example of Figure 15. Then, it suddenly disappears, and the periodic attractor becomes globally attracting.

This is a typical boundary crisis [4], and the underlying global bifurcation is the homoclinic bifurcation of the saddle associated with the periodic attractor (they are born together through a SN). This is clear from Figure 16, which reports the relevant manifolds and clearly shows the homoclinic tangency.

From the comparison of Figures 15 and 16 it is clear that the stable manifolds of the saddle are the boundary between the basins of competing attractors, and that the scattered chaotic attractor is shaped on the (right)

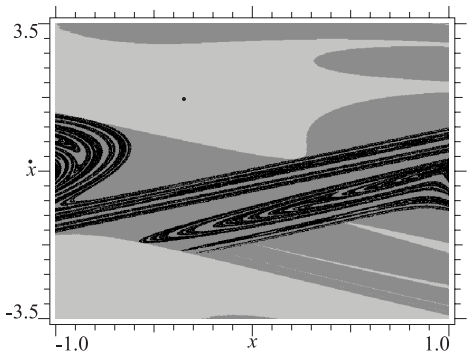

Figure 15: The scattered chaotic attractor just before the boundary crisis at $\gamma = 1.222$ and $\omega = 3$.

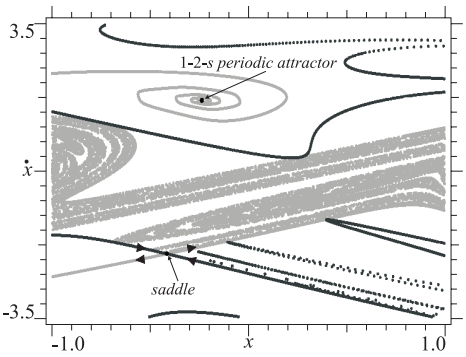

Figure 16: Stable and unstable manifolds of the saddle experiencing homoclinic bifurcation responsible for the boundary crisis at $\gamma = 1.22$ and $\omega = 3$.

unstable manifold of the saddle. Therefore, it is clear why this boundary crisis coincides with the homoclinic bifurcation of the saddle.

Curve (B). Curve (B) is just the curve γ_{cr}^{c}, introduced in Sect. 4, where chattering disappears. Further comments on this curve are postponed to point **(1)** below.

Curve (C). Along curve (C) there is the final crisis of the bifurcation diagram ensuing from the $1-1-c$ periodic attractor of Figure 7a, which is illustrated in detail in Figure 17 with reference to the case $\omega = 12$.

At the end of the PD cascade the small chaotic attractor evolves through successive close widenings due to merging-type interior crises (IC1) [19, 15] through which the attractor enlarges but remains "non-robust". This path ends with a bursting-type interior crisis (IC2) [4, 15] after which the robust, confined, chaotic attractor is definitely established.

The route to chaos illustrated in Figure 17 occurs in a very narrow interval of values of γ (see Figure 17c), so that, while maintaining theoretical interest, it is not very important from an engineering point of view and will not be further investigated.

Curve (D). Curve (D) corresponds to the homoclinic bifurcation γ_{cr}^{h} of the hilltop saddle, which has been studied in depth, e.g., in [7, 8]. In those papers it was shown that, for increasing excitation amplitude, the stable and

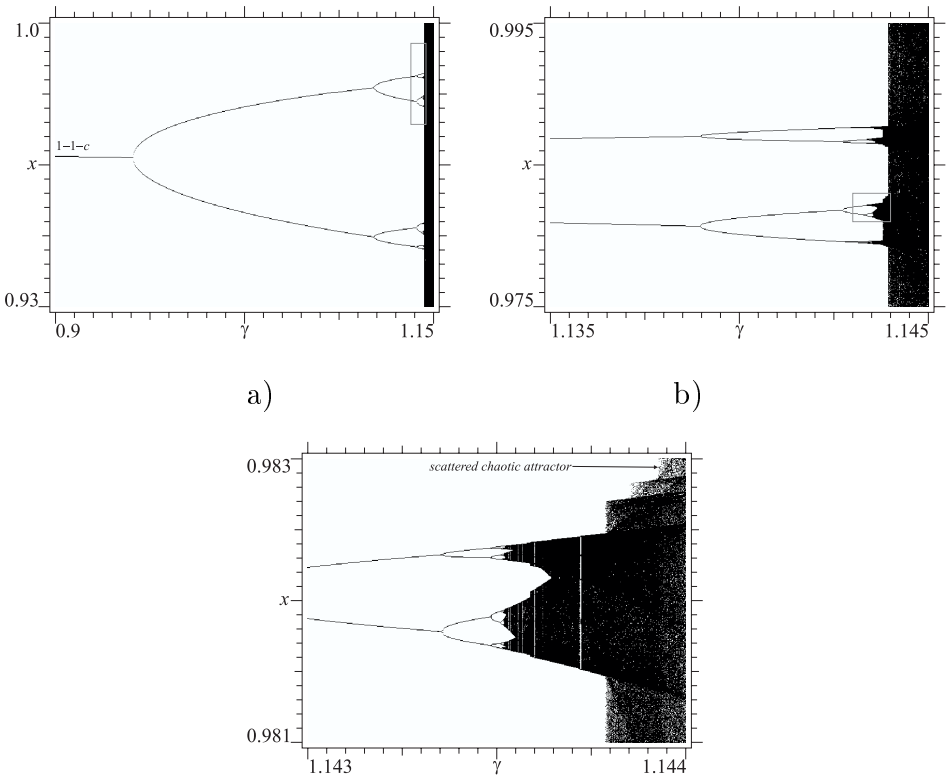

Figure 17: Successive enlargements of the bifurcation diagram ensuing from the $1-1-c$ periodic attractor at $\omega = 12$ across its final crisis.

unstable manifolds of the hilltop become tangent (see the following Figure 19) when γ reaches the critical value

$$\gamma_{cr}^{h} = \frac{[(1-r)\sqrt{1+\delta^2} + (1+r)\delta]\sqrt{(1+\omega^2)^2 + (2\delta\omega)^2}}{\sqrt{[(1-r)\sqrt{1+\delta^2} + (1+r)\delta]^2 + [\omega(1+r)]^2}}, \tag{8}$$

which is the analytical expression of curve (D). Below this threshold, the manifolds stay disjoint, thus preventing the onset of scattered robust chaotic attractors, while above it they intersect and thus create the chaotic saddle responsible for the chaotic transient, for the fractal basin boundaries and allowing for the scattered chaotic attractor (Figure 14).

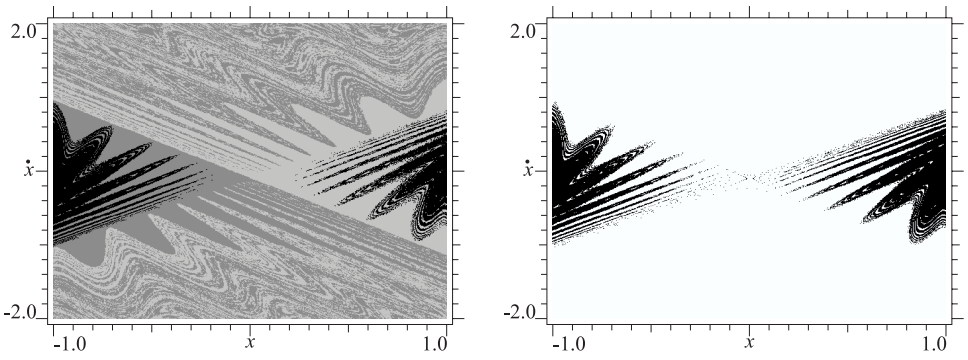

a) b)

Figure 18: a) Confined ($\gamma = 1.65$) and b) scattered ($\gamma = 1.8$) chaotic attractors across the homoclinic bifurcation threshold of the hilltop saddle. $\gamma = \gamma_{cr}^{h} = 1.656$ and $\omega = 18$.

When we approach the critical threshold (D), the confined chaotic attractor enlarges inside its basin until, for $\gamma = \gamma_{cr}^{h}$ it touches the basin boundary, as shown by the example of Figure 18a. Then, it merges with its symmetric counterpart giving a unique chaotic attractor spanning both potential wells (Figure 18b).

This phenomenon is a typical mechanism of transition from confined to scattered chaotic attractors occurring in symmetric systems and named merging-type symmetric boundary crisis (BCS) [5]. The underlying global bifurcation, i.e., already mentioned homoclinic bifurcation of the hilltop saddle, is illustrated in Figure 19, which clearly shows the tangencies of the manifolds.

From the comparison of Figures 18 and 19 it is clear that the stable manifolds are the boundary between the basins of competing confined chaotic attractors, which are shaped by the unstable manifolds. This shows why this symmetric boundary crisis coincides with the homoclinic bifurcation of the hilltop saddle.

Indeed, for γ only slightly larger than γ_{cr}^{h}, the onset of the scattered chaotic attractor requires an extremely long transient; for $\gamma = 1.75$ and $\omega = 18$, for example, it takes over 3×10^6 periods. This is the reason why the theoretical γ_{cr}^{h} and its numerical counterpart differ in Figure 13b, which

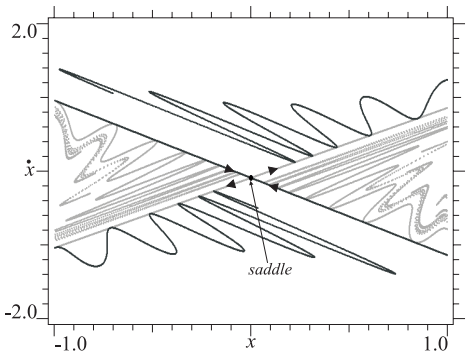

Figure 19: Stable and unstable manifolds of the hilltop saddle experiencing homoclinic bifurcation responsible for the symmetric boundary crisis at $\gamma_{cr}^{h} = 1.656$ and $\omega = 18$.

is simply due to the fact that the numerical bifurcation diagram is built by considering "only" 500000 periods to limit the CPU time.

From the previous considerations and from Figure 14, several conclusions can be drawn.

(1). Below γ_{cr}^{c} no chaotic attractors have been observed in our numerical simulations, and therefore it represents a lower bound for chaos. This confirms and extends conclusion (i) stated earlier in this Section.

The mechanism of how the rest positions and chattering oscillations inhibit chaos is not completely clear: we conjecture that this is due to the fact that robust chaotic attractors (both confined and scattered) occur on the unstable manifolds of the hilltop saddle. These manifolds, however, accumulate near $x \pm 1$, and thus drive trajectories towards the rest positions or chattering oscillations. Only when these attractors disappear the trajectories are free to wander all around the manifolds and, possibly, to give rise to the chaotic attractor.

(2). The (ω,γ) parameter space is basically divided in two zones with qualitatively different dynamical behaviour, one for $\omega < \omega_{cr}$ and the other for $\omega > \omega_{cr}$. Rigorously, ω_{cr} corresponds to the left vertex of the (light gray) region of the confined chaotic attractor, but from an engineering point of view it can be approximated by the frequency value where γ_{cr}^{c} and γ_{cr}^{h} intersect, as reported in Figure 14 ($\omega_{cr} \cong 10.8$).

This approximation permits to define small frequencies as those values of

ω for which the homoclinic bifurcation of the hilltop saddle occurs below the end of the rest position and chattering, and large frequencies those for which the opposite occurs.

(3). For small frequencies, only scattered chaotic attractors are possible, while for large frequencies confined chaotic attractors appear first. This confirms and extends conclusion (ii) stated earlier in this Section.

(4). For $\omega > \omega_{cr}$, the homoclinic bifurcation of the hilltop saddle assumes the very important role of the dynamical event leading from confined to scattered chaotic dynamics. An equivalent conclusion was drawn in Sect. 4 of Part I of [8] for $\delta = 0.2$, $r = 0.8$ and $\omega = 5$. Note that for this set of dissipation parameters the critical frequency is about $\omega_{cr} \cong 2.8$, so that $\omega = 5$ belongs to the region of large frequencies. These considerations further support our conclusions, and allow to assert that this type of behaviour is observed for both slightly and strongly damped systems.

(5). The region of scattered chaotic attractors is bounded from below by the threshold $\gamma^* = min\{\gamma^c_{cr}, \gamma^h_{cr}\}$, which is only an approximation around $\omega \approx \omega_{cr}$. An analytical engineering approximation of γ^* is $min\{1, \gamma^h_{cr}\}$ (see Remark 1).

(6). The appearance/disappearance, as well as the main topological changes, of the chaotic attractors are due to various kinds of boundary crisis, which can be interpreted in terms of homoclinic bifurcations of appropriate saddles. Of course, also heteroclinic bifurcations may play a role in other specific situations.

(7). The chaotic attractors of Figure 14 are in general not globally attracting, as is clearly shown by Figure 15 and by the periodic map in Figure 8. They can coexist with a periodic attractor, showing a different kind of multistability, which adds to the one discussed in Sect. 3. This confirms that multistability is a quite robust characteristic of the inverted pendulum with lateral barriers.

(8). In the chaotic region there are strips where a periodic attractor replaces the chaotic attractor. The most important one contains a $3-2-s$ attractor and is visible in Figure 14; other periodic windows have been encountered, but they are very narrow and are not shown in Figure 14. The transition from chaotic to periodic attractors in these windows is likely due to crises similar to those previously described.

6 Conclusions and further developments

A systematic investigation of the nonlinear dynamics of an inverted pendulum between lateral walls has been performed.

The periodic attractors scenario has been considered first, by studying the range of existence of the main stable cycles by the combined use of numerical basins of attraction and bifurcation diagrams. Attention was focused on local and global bifurcations that lead to appearance and disappearance of periodic attractors, and the relevant behaviour charts have been built.

The overall periodic attractors map has then been discussed and illustrated in detail, and it has been shown how, in a certain region of the parameter space, multistability of periodic attractors, of various period and both confined and scattered, is common, while in other regions only one cycle is observed. This provides a large flexibility in view of practical applications, since different regions of behaviour can be chosen, according to the required performances. Furthermore, coexistence of both periodic and robust chaotic attractors has been observed in significant parts of the parameter space.

The chattering behaviour appearing just at the end of the rest position is the main non-smooth phenomenon characteristic of this class of non-resonant oscillators. After qualitative considerations, a method has been proposed to compute the time length τ of chattering; this method also provides information on the disappearing of chattering as the excitation amplitude γ is increased. An asymptotic estimate of the singular behaviour of τ for $\gamma \to 1^+$ has been obtained.

Finally, the occurence of robust chaotic attractors, the third broad class of qualitatively different observed attractors, has been studied. An overall map of chaotic attractors has been obtained, and two different behaviours, one for small and one for large frequencies, have been described. The transition from confined to scattered chaotic attractors through a symmetric boundary crisis related to the homoclinic bifurcation of the hilltop saddle has been illustrated, as well as a boundary crisis leading to the sudden disappearance of a scattered chaotic attractor due to the homoclinic bifurcation of another saddle, different from the hilltop one.

Various developments of the present investigation can be sought for and appear worth being pursued. Among others, we mention a better understanding of the chattering behaviour, possibly by using abstract analytical tools [1], and the extension to more general excitations, which are more realistic and arise in the field of chaos control [7].

References

[1] Budd, C., and Dux, F., 1994, "Chattering and related behaviour in impact oscillators," *Phil. Trans. R. Soc. London A.* **347**, pp. 365-389.

[2] Chatterjee, S., Mallik, A.K., and Ghosh, A., 1995, "On impact dampers for non-linear vibrating systems," *J. Sound Vibr.*, **187**(3), pp. 403-420.

[3] Demeio, L., and Lenci, S., 2005, "Asymptotic analysis of chattering oscillations for an impacting inverted pendulum," In preparation.

[4] Grebogi, C., Ott, E., and Yorke, J. A., 1983, "Crises, Sudden Changes in Chaotic Attractors, and Transient Chaos," *Physica D*, **7**, pp. 181-200.

[5] Grebogi, C., Ott, E., Romeiras, F., and Yorke, J.A., 1987, "Critical Exponents for Crisis-Induced Intermittency," *Phys. Review A*, **36**, pp. 5365-5380.

[6] Knudsen, C., Feldberg, D., and True, H., 1992, "Bifurcations and Chaos in a Model of a Rolling Railway Wheelset," *Phil. Trans. Royal Soc. London*, **A338**, pp. 455-469.

[7] Lenci, S., and Rega, G., 1998, "A Procedure for Reducing the Chaotic Response Region in an Impact Mechanical System," *Nonlin. Dyn.*, **15**, pp. 391-409.

[8] Lenci, S., and Rega, G., 1998, "Controlling Nonlinear Dynamics in a Two-Well Impact System. Parts I & II," *Int. J. Bif. Chaos*, **8**, pp. 2387-2424.

[9] Lenci, S., and Rega, G., 2000, "Periodic Solutions and Bifurcations in an Impact Inverted Pendulum under Impulsive Excitation," *Chaos, Sol. Fractals*, **11**, pp. 2453-2472.

[10] Lenci, S., and Rega, G., 2003, "Regular Nonlinear Dynamics and Bifurcations of an Impacting System under General Periodic Excitation," *Nonlin. Dyn.*, **34**, pp. 249-268.

[11] Masri, S.F., Miller, R.K., Dehghanyar, T.J., and Caughey, T.K., 1989, "Active parameter control of nonlinear vibrating structures," *ASME J. Appl. Mech.*, **56**, pp. 656-666.

[12] Moore, D.B., and Shaw, S.W., 1990, "The Experimental Response of an Impacting Pendulum System," *Int. J. Non-linear Mech.*, **25**, pp. 1-16.

[13] Nordmark, A., 1991, "Non-periodic motion caused by grazing incidence in an impact oscillator," *J. Sound Vibr.*, **145**, pp. 279-297.

[14] Peterka, F., 1996, "Bifurcations and Transition Phenomena in an Impact Oscillator," *Chaos, Sol. Fractals*, **7**, pp. 1635-1647.

[15] Rega, G., and Salvatori, A., 1996, "Bifurcation Structure at 1/3-subharmonic Resonance in an Asymmetric Nonlinear Elastic Oscillator," *Int. J. Bif. Chaos*, **6**, pp. 1529-1546.

[16] Sadek, M.M., 1972, "Impact dampers for controllling vibration in machine tools," *Machinery*, **102**, pp. 152-161.

[17] Shaw, S.W., and Rand, R.H., 1989, "The Transition to Chaos in a Simple Mechanical System," *Int. J. Non-linear Mech.*, **24**, pp. 41-56.

[18] Shaw, S.W., 1990, "The Suppression of Chaos in Periodically Forced Oscillators," In *Nonlinear Dynamics in Engineering Systems, W. Schiehlen (ed.), Proc. of IUTAM Symposium, Stuttgart, Germany, August 21-25, 1989*. Berlin, Springer-Verlag, pp. 289-296.

[19] Sommerer, J.C., and Grebogi, C., 1992, "Determination of crisis parameter values by direct observation of manifold tangencies," *Int. J. Bif. Chaos*, **2**, pp. 383-396.

[20] Stephenson, A., 1908, "On Induced Stability," *Phylosophical Magazine*, **15**, pp. 233-236.

[21] Wiercigroch, M., and Budak E., 2001, "Sources of nonlinearities, chatter generation and suppression in metal cutting," *Phil. Trans. R. Soc. London A*, **359**, pp. 663-693.

[22] Zhao, X., Dankowicz, H., Reddy, C.K., and Nayfeh, A.H., 2004, "Modelling and simulation methodology for impact microactuators," *J. Micromech. Microeng.*, **14**, pp. 775-784.